Chapter 9
Model Updating Technique for Modal Shaker Modeling

Abraham Ramirez, Peter Fickenwirth, John Schultze, and Shannon Danforth

Abstract Electrodynamic shakers are commonly used in the shock and vibration testing field, but despite their commonality, a proper characterization of their dynamics is often unknown. An improved understanding of these shakers can help inform test engineers on the feasibility of achieving a test specification, which will help to reduce delays and improve selection of test equipment. The work presented here is a unique approach to numerically estimate lumped model parameters based on the system's experimental frequency response functions (FRFs). The model parameters were then optimized to reduce the normalized root mean squared error between modeled and experimental responses. The similarity between the modeled FRFs and the experimental FRFs was then presented. This updating technique provides a method to predict the experimental FRFs of the shaker given differing environments and test object masses, thus aiding test engineers in determining test feasibility.

Keywords Electrodynamic shaker · Vibration testing · Modal testing · Model Updating, Optimization

Introduction

Environmental testing is a necessary step to qualify that a system will continue to work as intended during and after it is subjected to dynamic loads that it will see throughout its lifetime. One part of this environmental testing is vibration and shock testing, which most commonly uses electrodynamic shakers. During a vibration test, the response of the device under test (DUT) is monitored and the output level of the shaker is adjusted to meet a pre-specified power spectral density (PSD) function. Historically, shakers are selected based similarity to past tests, engineering judgement, and simple calculations using Newton's second law of physics. However, the electrodynamic shaker systems used to perform these tests have complicated dynamics, and there are many variables to consider when predicting a system's capability. Having a more detailed understanding of these capabilities would allow the test engineers to predict test limitations and better utilize the equipment available.

Electrodynamic shakers can be be modeled by solving a representative multi degree of freedom (DoF) lumped parameter model. The model includes both mechanical and electrical components, and uses a coupling coefficient that serves to couple the dynamics of the mechanical system to the electrical system. A few of the model parameters can be directly measured or are provided by the shaker manufacturer, but the remaining model parameters must be estimated. Previous work has shown that this method for modeling electrodynamic shakers is promising [1], but this approach requires a large amount of manual tuning and was applied to only larger, fixed-base shakers. One suitable method for reducing the amount of manual tuning is to use experimentally identified natural frequencies and knowledge of the shaker's mode shapes. A further improvement to the model fidelity may then be achieved by using an error reduction optimization.

This paper builds on previous shaker modeling work by applying the method described above to modal shakers and improving performance in frequency ranges with poor experimental prediction accuracy. First, we provide an introduction to electrodynamic shaker construction and dynamics. Next, we introduce our model of the electrodynamics shakers used in this study and detail the methods for modal parameter identification. We then introduce an optimization algorithm that identifies frequency ranges where the model performed poorly, determines which model parameters affected performance, and varies those parameters only in the identified frequency ranges. This paper will be primarily focused on smaller modal shakers as opposed to larger fixed base shakers. Our comparison to experimental results shows that the method proposed in this paper for estimating the model parameters yielded predicted FRFs that represented the true system dynamics well.

Abraham Ramirez · Peter Fickenwirth · John Schultze · Shannon Danforth
Los Alamos National Laboratory
e-mail: ajrami@umich.edu; petefickenwirth@gmail.com; schultze@lanl.gov; sdanforth@lanl.gov

Brandon Dilworth et al. (eds.), *Topics in Modal Analysis & Parameter Identification I, Vol. 9*, Conference Proceedings of the Society for Experimental Mechanics Series, https://doi.org/10.13052/97887-438-0154-2_9

Electrodynamic Shaker Construction and Modes

The basic functionality of an electrodynamic shaker comes from a coil that is suspended in a fixed magnetic field and is passed an alternating current. When this current is passed through a coil that is wrapped around the armature, a magnetic field is created. The interaction between the fixed magnetic field and the induced electromagnetic field of the coil create axial vibrations on the armature [2].

The coil is made from heavy conductors that allows a large amount of current to flow through. The flexures comprise the suspension system that suspends the armature and coil in the magnetic field. These flexures allow axial motion and limit all other motion. The magnets create the fixed radial magnetic field. Lastly, the stinger is a thin rod that is attached to the shaker by a collet and is used to transfer excitations to a device under test (DUT). A visual representation of these parts is shown in Fig. 1, as proposed by Schultz [3].

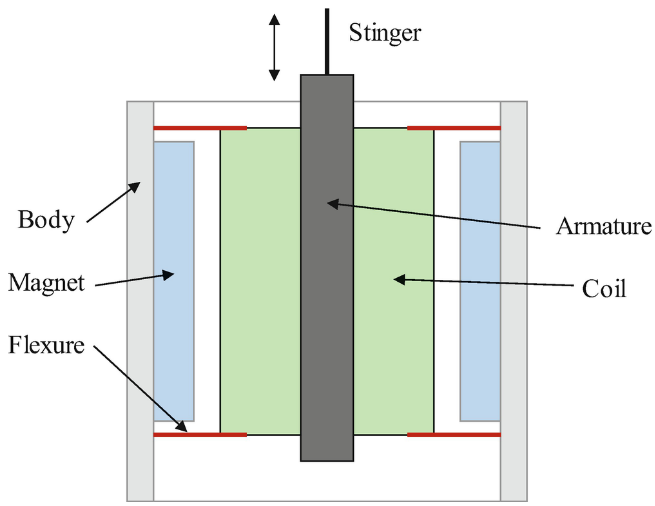

Fig. 1 Electrodynamic shaker design.

Due to this construction, shakers typically display two modes of vibration:

1. **Suspension mode**: Armature, coil and flexures move opposite the body, low frequencies (10 - 30 Hz).
2. **Stinger mode**: Stinger moves opposite the armature, high frequencies (1500 - 4500 Hz).

A depiction of the mode shapes of both modes are seen in Fig. 2. A sample stinger acceleration over current FRF of the system shows two 90° phase shifts that correspond to the two modes in Fig. 3.

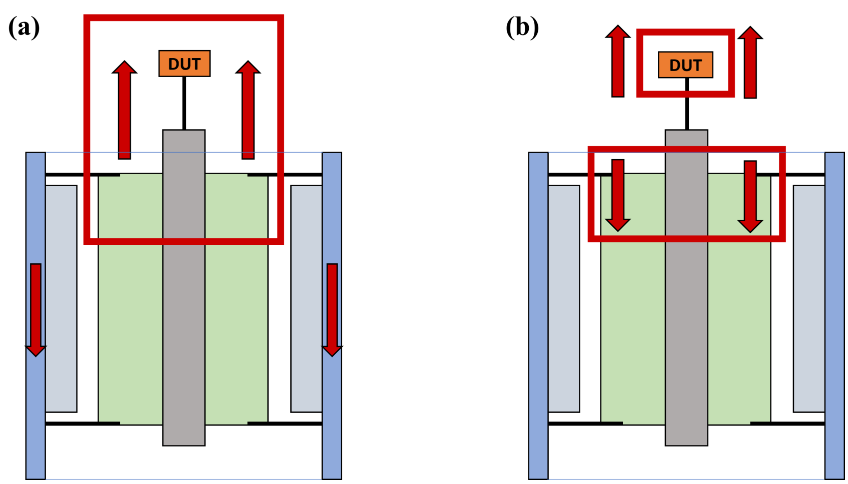

Fig. 2 Modal shakers vibration modes. (a) Suspension mode. (b) Stinger mode.

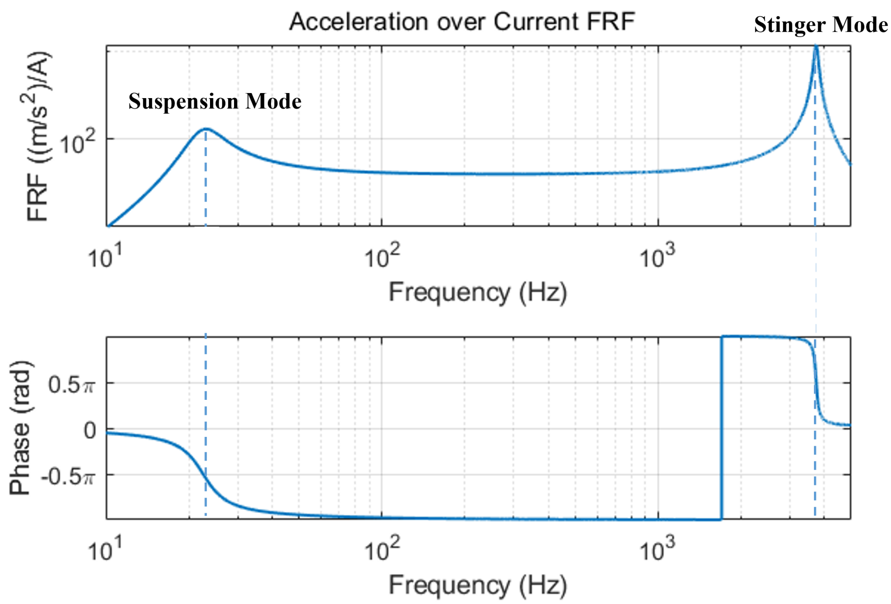

Fig. 3 Acceleration over current frequency response showing peaks and phase shifts correlating to vibration modes.

It is worth noting that at very low frequencies, there is another mode called the isolation mode. At this mode, the entire body of the shaker moves axially as a rigid body. Since it is very rare to encounter this mode in practice, it is not considered in this work.

Shaker Limitations

Shakers have differing limitations across frequency ranges that are commonly tested [2]. In general, at low frequencies the shaker is limited by the maximum stroke length and/or the maximum root mean squared (RMS) voltage of the amplifier. Then, just past the suspension mode frequency in the flat region of the acceleration over current FRF, the shaker is limited by the maximum RMS current of the amplifier. At high frequencies in the region sloping up to the coil mode, the shaker is limited mechanically by maximum armature force rating. Lastly, for anything beyond the force-limiting range, the shaker is limited again by the maximum RMS voltage capability of the amplifier. A representation of the the limitations across the frequency range can be seen in Fig. 4.

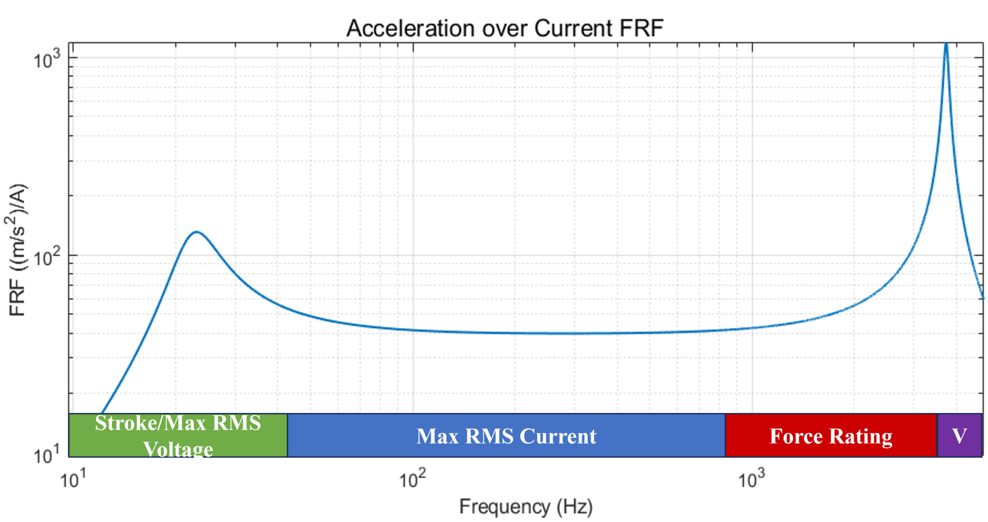

Fig. 4 Shaker limitations on frequency response magnitude plot.

The values of the shaker's natural frequencies are subject to changing test conditions. These changing conditions include the DUT mass, orientation of the shaker, stinger length, and stinger thickness. This shift in natural frequencies then changes where the aforementioned limitations occur in the frequency range. Knowledge of the shaker limitations and the frequency ranges of each limitation is valuable information for a test engineer in the planning and execution stages of a test.

Electromechanical Lumped Parameter Model

Many different ways of modeling a shaker using an equivalent lumped parameter model have been proposed. Most of the work has been focused on modeling fixed-base shakers, which have different dynamics when compared to smaller modal shakers. For fixed-base shaker modeling, Tiwari et al. laid out a framework for using an equivalent electrical (RLC) circuit and ways to reduce the corresponding impedance expression in order to numerically estimate the model parameters using experimental data [4]. Other work for modeling fixed-base shakers used an equivalent mechanical system (MCK) coupled to an electrical circuit with a coefficient that links the electrical and mechanical DoFs [1][5][6]. Schultz used a similar equivalent electromechanical model, but focused on modeling the electrical impedance of modal shakers [3]. The limitation of modeling only the impedance is that the impedance is a ratio of electrical signals, which can hide inaccurate acceleration amplitudes. Thus, only analyzing the modeled impedance may not be advantageous in providing the test engineer with a true representation of the system.

In this study, we use similar techniques to Martini, but apply the methodology to modal shakers rather than fixed base shakers. The model used in this study is a representative electromechanical model consisting of two mechanical DoFs and one electrical DoF with a coupling coefficient, as seen in Fig. 5.

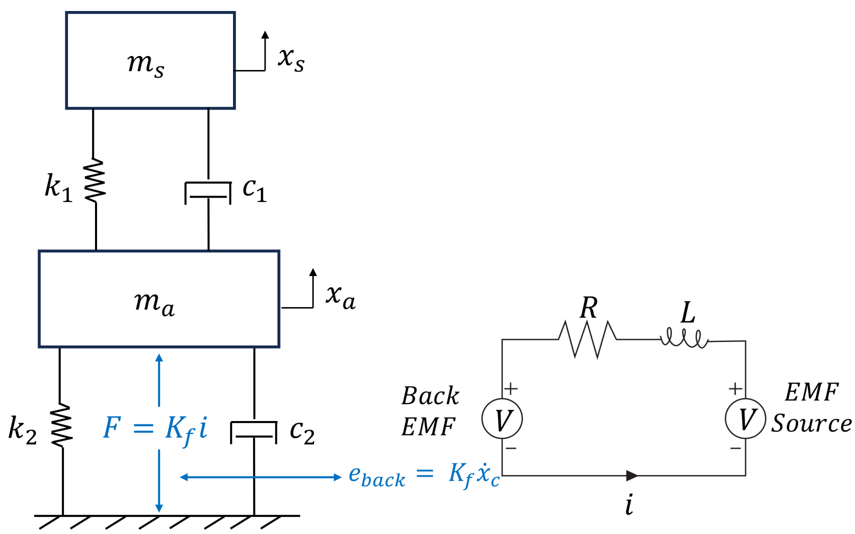

Fig. 5 Combined electromechanical lumped parameter model.

The mass m_a represents the mass of the armature, and m_s represents the mass of the stinger and relative DUT mass. The stiffness and damping of the flexures are represented by k_2 and c_2, respectively. Similarly, the stiffness and damping of the stinger are represented by k_1 and c_1, respectively.

The electrical system is represented by a voltage source, resistor, and inductor all in series. There is another voltage source that is representative of the back electromotive force (EMF). This back EMF is a voltage that is generated by the relative velocity of the coil within the magnetic field. The back EMF subtracts from the voltage generated by the amplifier and is greatest at lower frequencies when the coil has higher displacements. At high frequencies, the motion of the coil is negligible and the back EMF is therefore also negligible. This coupling is represented by the coefficient K_f, which is equal to the magnetic field strength, B, multiplied by the total coil length, l. This coefficient couples the current in the electrical domain to the motion of the coil in the mechanical domain. A visual of this coupling may be seen in Fig. 6 as depicted in the H560 shaker manual by Unholtz-Dickie Corporation [7].

From this model, a set of equations of motions may be formed. Each DoF has its own equation, meaning that there are two mechanical equations of motion and one electrical equation of motion. A block matrix representation is shown below:

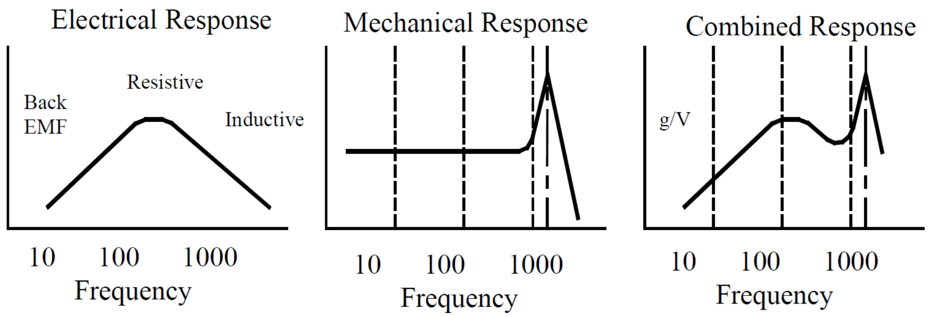

Fig. 6 Visual of the coupling between the electrical and mechanical systems.

$$\begin{bmatrix} m_s & 0 & 0 \\ 0 & m_a & 0 \\ 0 & 0 & 0 \end{bmatrix} \begin{Bmatrix} \ddot{x_s} \\ \ddot{x_a} \\ \ddot{i} \end{Bmatrix} + \begin{bmatrix} c_1 & -c_1 & 0 \\ -c_1 & c_1 + c_2 & 0 \\ 0 & -K_f & L \end{bmatrix} \begin{Bmatrix} \dot{x_s} \\ \dot{x_a} \\ \dot{i} \end{Bmatrix} + \begin{bmatrix} k_1 & -k_1 & 0 \\ -k_1 & k_1 + k_2 & K_f \\ 0 & 0 & R \end{bmatrix} \begin{Bmatrix} x_s \\ x_a \\ i \end{Bmatrix} = \begin{Bmatrix} 0 \\ 0 \\ E \end{Bmatrix}$$

Lumped Model Parameter Identification

As mentioned previously, only a few of these parameters are provided or are easily measurable. The masses may be found by either information provided in the shaker manual (m_a) or by measurement (m_s). A method to determine the remaining mechanical parameters is to utilize knowledge of the shaker modes to make simplified transfer functions. Using these simplified transfer functions the experimentally identified natural frequencies and magnitudes may be used to estimate the stiffness, damping, and coupling coefficient values.

The transfer function of the whole mechanical system is identified by taking the Laplace transform of both equations of motion, eliminating x_a by substitution, and rearranging in the form of stinger acceleration over current. This equation can be seen below:

$$H_{x_s,i} = \frac{X_s s^2}{I} = \frac{K_f(k_1 + c_1 s)s^2}{s^4(m_s m_a) + s^3(m_s(c_1 + c_2) + m_a c_1) + s^2(m_s(k_1 + k_2) + m_a k_1 + c_1 c_2) + s(k_1 c_2 + k_2 c_1) + k_1 k_2} \tag{1}$$

Coupling Coefficient Estimation

We estimate the coupling coefficient, K_f, by inspecting the magnitude of experimental stinger acceleration over current frequency response away from any influence of the suspension or stinger modes. We chose to analyze the magnitude of the response at 10x the suspension mode. The simplified transfer function for this case is given by

$$H_{x_s,i}(10 * f_{Sus.m}) = \frac{K_f}{m_a + m_s}. \tag{2}$$

Rearranging to solve for K_f gives

$$K_f = (m_a + m_s) \mid H_{x_s,i}(10 * f_{Sus.m}) \mid . \tag{3}$$

Low Frequency Simplifications

As discussed in the Electrodynamic Shaker Construction and Modes section, the transfer function may be simplified by leveraging knowledge of the shaker's modes. At low frequencies near the suspension mode, the armature and stinger move as one rigid mass. Thus, the model may be simplified to a one DoF system as seen in Fig. 7.

The stinger acceleration over current transfer function at low frequencies then becomes

$$H_{x_s,i_{LF}} = \frac{K_f s^2}{s^2(m_a + m_s) + sc_2 + k_2}. \tag{4}$$

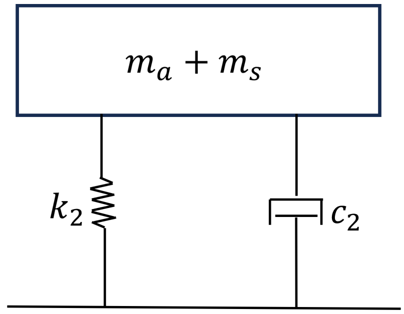

Fig. 7 Low frequency simplified mechanical model.

We can then use Eq. 4 to solve for the system's natural frequency near the suspension mode, given by

$$f_{Sus.M} = \frac{1}{2\pi}\sqrt{\frac{k_2}{m_a + m_s}}. \tag{5}$$

From Eq. 5, the flexure stiffness, k_2, can be solved for by using the experimentally identified suspension mode natural frequency and the known masses

$$k_2 = (2\pi * f_{Sus.M})^2(m_a + m_s). \tag{6}$$

Now, to solve for the flexure damping, c_2, Eq. 4 may be used. It is known that at a natural frequency the sum of the real parts of the frequency response approach zero. So the transfer function turns into to

$$H_{x_s,i_{LF}} = \frac{K_f s}{c_2}. \tag{7}$$

Rearranging Eq. 7 gives the following expression for flexure damping,

$$c_2 = \frac{K_f s}{\mid H_{x_s,i}(f_{Sus.M}) \mid} = \frac{K_f(2\pi * f_{Sus.M})}{\mid H_{x_s,i}(f_{Sus.M}) \mid}. \tag{8}$$

High Frequency Simplifications

Similar to the low-frequency simplifications, we simplify the model at high frequencies based on knowledge of the behavior of the stinger mode. At high frequencies, the flexures have very little influence on the response of the shaker. Therefore, we reduce the model such that the armature mass and stinger mass are connected to each other only by k_1 and c_1. This assumption then reduces the model to the two DoF model that is shown in Fig. 8.

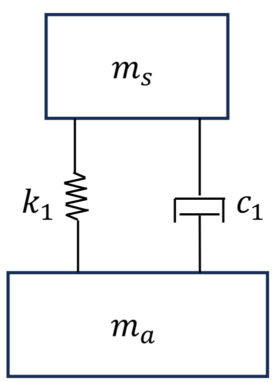

Fig. 8 High frequency simplified mechanical model.

Based on this model, the stinger acceleration over current transfer function at high frequencies may be represented as

$$H_{x_s,i_{HF}} = \frac{K_f(k_1 + c_1 s)}{s^2(m_a m_s) + s(c_1(m_s + m_a)) + k_1(m_s + m_a)}. \tag{9}$$

From Eq. 9, the natural frequency of the system may be represented as

$$f_{St.M} = \frac{1}{2\pi}\sqrt{\frac{k_1(m_s + m_a)}{m_a m_s}}. \tag{10}$$

Now, from Eq. 10 the stinger stiffness, k_1, may be solved for using the experimentally identified stinger mode frequency and the known masses

$$k_1 = (2\pi * f_{St.M})^2 \frac{m_s m_a}{m_s + m_a}. \tag{11}$$

Similar to the low-frequency case, to solve for the stinger damping, c_1, the high-frequency transfer function is reduced to

$$H_{x_s,i_{HF}} = \frac{K_f(c_1 s + k_1)}{s(c_1(m_s + m_a))}. \tag{12}$$

In order to isolate c_1, the fraction in Eq. 12 may be broken up to

$$H_{x_s,i_{HF}} = \frac{K_f c_1 s}{s(c_1(m_s + m_a))} + \frac{K_f k_1}{s(c_1(m_s + m_a))}. \tag{13}$$

From here, the $c_1 s$ in the first fraction of Eq. 13 may be cancelled and leaves

$$H_{x_s,i_{HF}} = \frac{K_f}{m_s + m_a} + \frac{K_f k_1}{s(c_1(m_s + m_a))}. \tag{14}$$

Lastly, because it is known that $k_1 >> K_f$, the term with the k_1 term will dominate the response. Thus for simplicity, the first fraction in Eq. 14 with K_f in the numerator is considered to be negligible. Then the equation can be reduced and used to solve for c_1 using

$$c_1 = \frac{K_f k_1}{(m_s + m_a)s \mid H_{x_s,i}(f_{St.M}) \mid} = \frac{K_f k_1}{(m_s + m_a)(2\pi * f_{St.M}) \mid H_{x_s,i}(f_{St.M}) \mid}. \tag{15}$$

Electrical Parameters

The two remaining parameters to be identified are the two electrical parameters; R and L. The resistance is given nominally in the shaker manual as approximately 1 ohm. This resistance value was then verified experimentally. As for the inductance, an initial value was simply estimated and tuned manually until the model closely matched the experimental data.

Optimization of Model Parameters

It is important to note that the Lumped Model Parameter Identification section lays out a methodology for *estimating* the model parameters. The reason it is only an estimation is because the previously simplified lumped parameter model was further reduced using knowledge of the shaker's modes. These simplifications were made so it was possible to mathematically solve for the model parameters. To further improve the model, an optimization of the parameters may be performed to reduce the model error. To do this, we inspect model predictions and experimental results while investigating the model's sensitivity to different experimental parameters. To understand the model parameter sensitivities, we plotted the stinger acceleration over current and stinger acceleration over voltage FRFs with each parameter at the estimated value, 0.5x estimated, and 2x estimated. Figure 9 shows a sample parameter sensitivity plot where k_2 was varied.

Recall one of the goals of this work was create a methodology for optimizing the modeled FRFs to improve the model in frequency ranges where it previously performed poorly. Therefore, the most important information to pull from the parameter sensitivity study is where in the frequency range a certain parameter affects the model. A summary of all the model parameter sensitivities can be seen in Table 1. This is so that when building the optimization, parameters are only varied in the frequency range in which they affect the model. This aids in minimizing parameters conflicting with one another during the optimization. As a result, a more accurate representation may be found and the overall optimization time is decreased.

The objective function used in this optimization is a normalized RMS error between the model and experimental data, similar to what was presented previously by Fickenwirth [1]. The normalization is done because the magnitude of the current driven response is much higher than the voltage driven response, thus the current driven response would dominate the error.

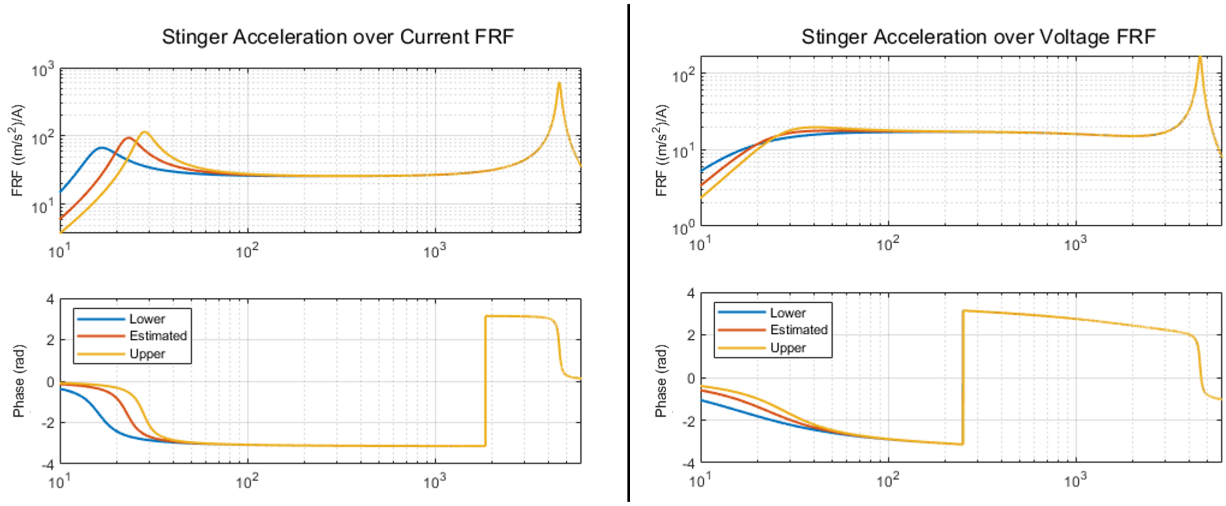

Fig. 9 Model sensitivity to flexure stiffness. Acceleration over current (left) and acceleration over voltage (right).

Table 1 Summary of parameter sensitivities

Parameter	**Effect of Increasing the Estimate on Acceleration over Voltage FRF**	**Effect of Increasing the Estimate on Acceleration over Current FRF**
m_s - Stinger mass	Decreases stinger mode frequency	Decreases stinger mode frequency
m_a - Armature mass	Decreases suspension and stinger mode frequencies, decreases overall amplitude	Decreases suspension and stinger mode frequencies, decreases overall amplitude
c_1- Stinger damping	Decreases coil mode amplitude	Decreases coil mode amplitude
c_2 - Flexure damping	Decreases suspension mode amplitude	Decreases suspension mode amplitude
k_1 - Stinger stiffness	Increases stinger mode frequency	Increases stinger mode frequency
k_2 - Flexure stiffness	Increases suspension mode frequency	Increases suspension mode frequency
K_f - Coupling coeff.	Increases overall amplitude	Increases overall amplitude
R - Resistance	Decreases overall amplitude	No effect
L - Inductance	Decreases amplitude near stinger mode	No effect

This magnitude difference is because the voltage driven response is heavily effected by the electromagnetic damping from the cross-coupling term, and the current driven response is not. The equation for the RMS error is

$$RMSE_{FRF} = \sqrt{\frac{\sum_{n=1}^{N} \sum (real(h_{n,model}) - real(h_{n,measured}))^2}{N}}. \tag{16}$$

In Eq. 16, h_n is the value of the frequency response at the n^{th} frequency line and N is the total number of spectral lines. There are a few different ways to normalize RMS error [8]:

1. **mean**: $NRMSE = \frac{RMSE}{\bar{y}}$
2. **range**: $NRMSE = \frac{RMSE}{y_{max} - y_{min}}$
3. **standard deviation**: $NRMSE = \frac{RMSE}{\sigma}$

For the purpose of this work the mean normalization was used. Then the total error is then represented as

$$error = NRMSE_{Accel/Voltage} + NRMSE_{Accel/Current}. \tag{17}$$

This objective function is then minimized using MATLAB's fmincon algorithm. Fmincon is a constrained nonlinear optimizer that finds the minimum of a scalar function starting at an initial estimate.

Experiment and Results

As described in section 4, we conduct the estimation using the natural frequency peaks from the acceleration over current FRF. In order to get these measurements, we threaded an impedance head onto the end of the stinger to measure acceleration. We monitored current from the amplifier's built in current monitor and measured the voltage supplied to and from the amplifier. These measurements were taken to be used later in calculating the acceleration over voltage FRF, which is used for further model comparison. The acceleration over voltage FRF was also used in the objective function for the optimization. For this work, the 2060E shaker from The Modal Shop was used. The test was a continuous random vibration test from 10-6000 Hz. Figure 10 shows the test setup.

Fig. 10 Experimental test setup.

Initial Estimates of Model Parameters

Using the collected experimental data, we calculated the frequency responses and identified the natural frequencies corresponding to the suspension mode and stinger mode, as shown in Fig. 11. These natural frequencies are listed in Table 2.

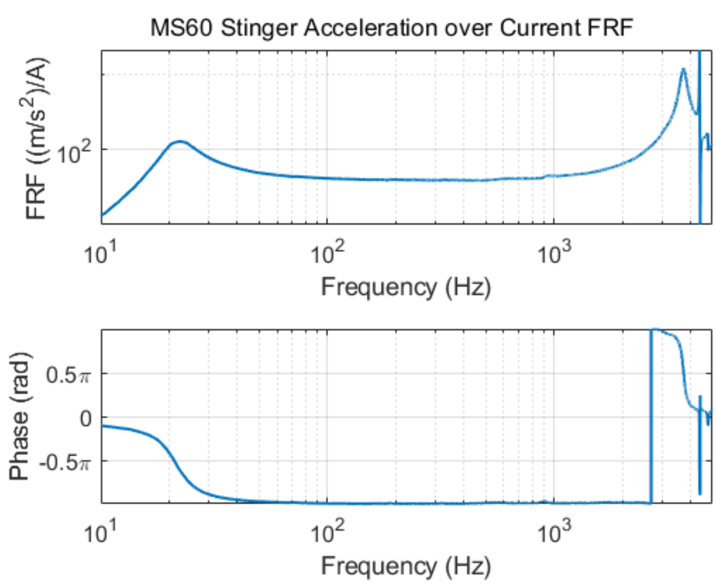

Fig. 11 Experimental acceleration over current FRF.

Table 2 Experimentally identified natural frequencies.

Mode	Symbol	Frequency (Hz)
Suspension	$f_{Sus.M}$	22.5
Stinger	$f_{St.M}$	3731.5

We then used the two natural frequencies to estimate the model parameters using the equations from section 4. The estimated model parameters are shown in Table 3. These estimated parameters are then plugged into the block matrix representation of the system and the direct frequency response method is used to calculate the modeled FRFs. [1].

Table 3 Estimated model parameters.

Model Parameter	Symbol	Initial Estimate	Unit
Stinger stack mass	m_s	0.038	kg
Armature mass	m_a	0.27	kg
Stinger damping	c_1	25.6	N/(m/s)
Armature Damping	c_2	13.4	N/(m/s)
Stinger stiffness	k_1	1.92E7	N/m
Armature Stiffness	k_2	6.16E3	N/m
Coupling Coefficient	K_f	12.2	-
Resistance	R	2	Ohms
Inductance	L	1e-4 - 1i*9e-7	Henry

$$H = (-\omega^2[M] + j\omega[C] + [K])^{-1} \tag{18}$$

Eq. 18 is calculated at each frequency line and forms the frequency response matrix, H, which is a $3x3xn$ matrix where n is the number of frequency lines. As described in section 3, the only force acting on the system is the applied voltage from the amplifier. This means that only the last column, which are the responses to a voltage reference, are needed to compare the model to the experimental results. The stinger acceleration over voltage FRF data is found in row 1 and the current over voltage FRF data is found in row 3. The modeled acceleration over current FRF is found by taking the reciprocal of the current over voltage FRF (also called the impedance) and multiplying by the acceleration over voltage FRF. The comparison of the estimated model (prior to any optimization) to the experimental results are shown in Fig. 12 and Fig. 13.

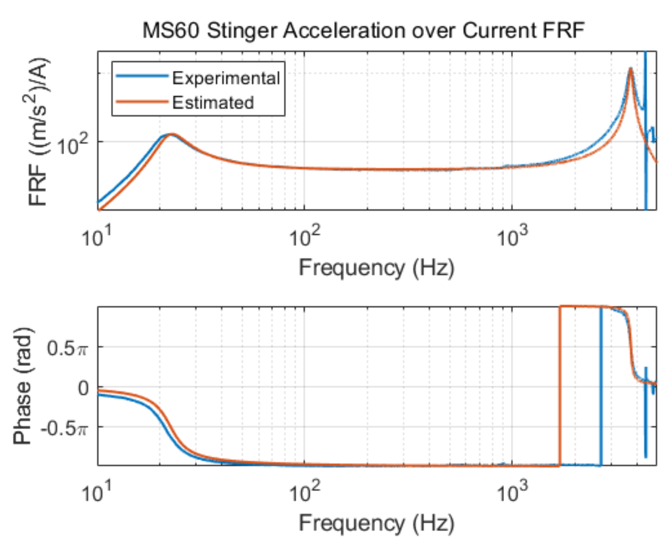

Fig. 12 Comparison for estimated model vs experimental acceleration over current FRFs.

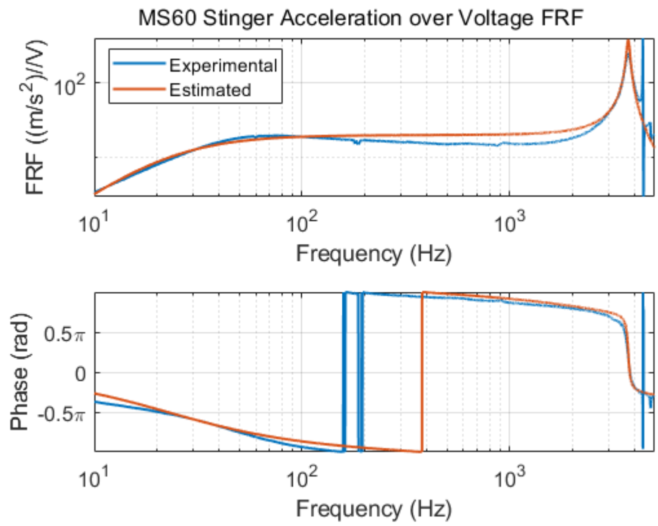

Fig. 13 Comparison for estimated model vs experimental acceleration over voltage FRFs.

Optimizing Model Parameters

Using the initial estimates as initial values, the optimization described in section 5 was formulated by: (1) Following the order of operations laid out by Schultz [3] and (2) Identifying the frequency range in which each variable is most effective, using the parameter sensitivity study as a starting point. The following shows the order of operations mentioned prior:

1. Optimize k_2 and k_1 to match the frequencies of the suspension and stinger modes, respectively.
2. Optimize L to match the curvature of the experimental acceleration over voltage FRF.
3. Optimize c_2 and c_1 to match the amplitudes of the suspension and stinger modes, respectively.
4. Optimize K_f to match the amplitude in the region between the two modes in the acceleration over current FRF.

Then by inspection of the FRF comparisons, each variable was given a specific frequency range in which it was most effective. For example, it is known from the parameter sensitivity study that the suspension stiffness, k_2, affects the model most near the suspension mode. Thus, k_2 was varied by only minimizing the error calculated between 10-30 Hz. A similar process was then followed for the rest of the variables. Table 4 shows how the optimization changed the model parameters. It should be noted that the masses were not varied.

Table 4 Comparison of estimated vs optimized variables.

Model Parameter	Symbol	Initial Estimate	Optimized	Unit
Stinger stack mass	m_s	0.038	0.038	kg
Armature mass	m_a	0.27	0.27	kg
Stinger damping	c_1	25.6	28.9	N/(m/s)
Armature damping	c_2	13.4	12.4	N/(m/s)
Stinger stiffness	k_1	1.92E7	1.92E7	N/m
Armature stiffness	k_2	6.16E3	5.55E3	N/m
Coupling coeff.	K_f	12.2	12.2	-
Resistance	R	2	2.15	Ohms
Inductance	L	1E-4 - 1i*9E-7	1.37E-4 - 1i*2.56E-5	Henry

Figures 14 and 15 shows a visual comparison between the initial estimated values and the optimized values to the experimental values.

A quantitative analysis of the similarity between the experimental and the estimated and optimized respectively was performed by calculating the RMS value of the decibel (dB) error at every frequency line [9]. This metric was chosen because it is calculated on a log scale, meaning that it weighs each point equally. Other metrics such as % RMS error favor

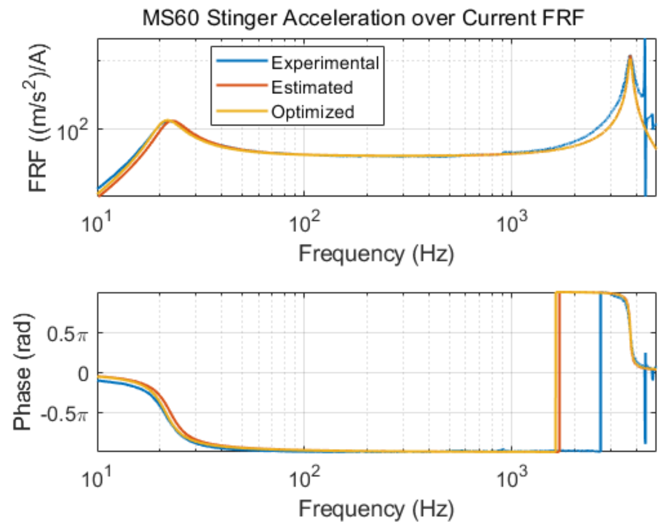

Fig. 14 Comparison of estimated vs optimized parameters for the acceleration over current FRF.

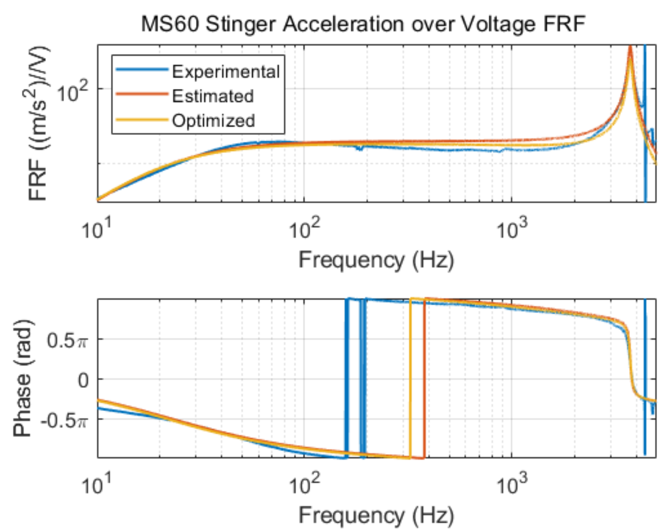

Fig. 15 Comparison of estimated vs optimized parameters for the acceleration over voltage FRF.

error at higher magnitudes more than low magnitude error, which can skew the total error. The formula for the RMS dB error metric is

$$RMSdB : \delta = \sqrt{\frac{1}{nf}\sum_{i=1}^{nf}\frac{1}{na}\sum_{k=1}^{na}[[log_{10}\beta_A(\omega)] - [log_{10}\beta_B(\omega)]]^2}. \tag{19}$$

$\beta_A(\omega)$ = Signal 1
$\beta_B(\omega)$ = Signal 2
nf = number of frequencies
na = number of channels
δ = error scalar

The results of the RMS dB error calculations are shown in table 5. These values are meant to compare the relative similarity between the modeled FRFs and the experimental FRFs. These calculations are single data comparisons for the acceleration over current FRFs and the acceleration over voltage FRFs, respectively.

Table 5 Model RMSdB error values of estimated values and optimized values.

	Initial Estimates	Optimized
A/C FRF RMS dB Error	26.864	27.785
A/V FRF RMS dB Error	12.210	10.416

Discussion

Overall it is seen that the lumped parameter model is highly representative of the real system. The initial values that used the acceleration over current FRF to estimate the parameters performed well. Due to this performance of the initial estimate, the optimization improvements are slight. This improvement can be observed qualitatively by inspection of figures 14 and 15 and by looking at the RMS dB error values in table 5. The two main areas of improvement are: (1) an improved alignment of the suspension mode frequency in the acceleration over current FRF, (2) overall improved amplitude prediction at the stinger mode for both FRFs. Elaborating more on the stinger mode amplitude improvement, Fig. 16 shows a zoomed in comparison for the stinger mode peak on both acceleration over current and acceleration over voltage FRFs.

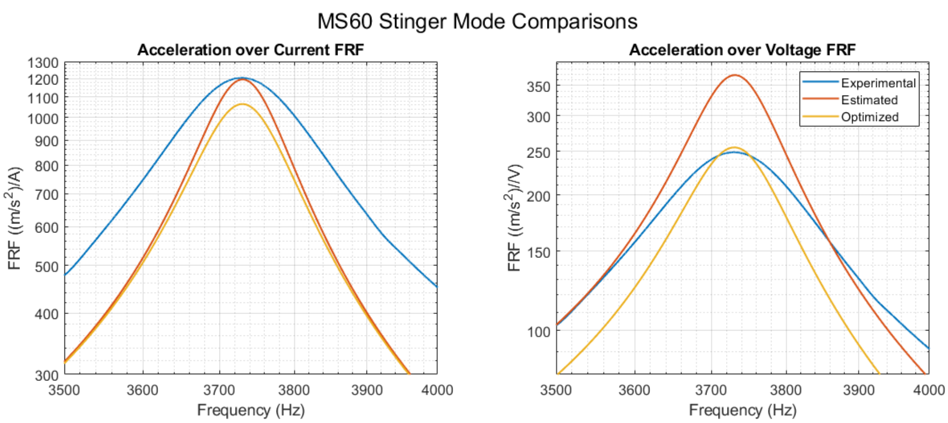

Fig. 16 Zoomed in view of stinger mode on both acceleration over current and acceleration over voltage FRFs.

Due to the initial estimate being done using the experimental acceleration over current FRF, it is reasonable that the model aligns at the stinger mode peak for the acceleration over current FRF prior to optimization. As a result, the acceleration over voltage FRF is over-predicting the stinger mode peak. Thus, the optimization resulted in the acceleration over current FRF increasing in error near the stinger mode peak and decreasing the error near the stinger mode peak for the acceleration over voltage FRF. The quantitative similarity comparison agrees with this visual observation. As the acceleration over voltage FRF's RMS dB error decreased due to the optimization, the acceleration over curent FRF's RMS dB error was increased. It should be noted that the RMS dB error was only calculated from 10-4000 Hz because the experimental data had an unusual sharp peak around 4100 Hz that is likely not a mechanical response but rather an error in the measurement for the electrical signals.

Conclusions

The aim of this study was to formulate an approach to estimate lumped model parameters that are representative of modal shakers. Overall, the proposed methods require only a small data set that yields a highly representative model. This approach may also be applied to many other modal shakers that share a similar construction to the one used for the experimental work used in this paper. Although the methods were shown to be successful, further improvements may still be made. Modal shakers dynamics are highly dependent on changing test conditions. These conditions include stinger length, stinger thickness, mass loading, boundary conditions, and orientation. For example, changing the stinger length will tend to decrease the stinger stiffness and will shift the stinger mode natural frequency down as a result. The methods described in this paper are not highly robust to these changing test conditions. This means that the shaker model estimations will need to be made using data that comes from a shaker in similar conditions to what the test engineers believes it will be used in the real test.

The improved shaker modeling method described in this paper can be used in dynamic substructuring to couple the shaker's dynamics to the dynamics of a device under test. This coupled model can then predict test feasibility by obtaining the required electrical inputs from the amplifier, which makes up a large portion of the shaker's limitations as described in Shaker Limitations section. Having this information that aids in determining test feasibility will ultimately help to reduce delays and improve the overall efficiency of ground environmental test series.

Acknowledgments This work was funded by the Delivery Environments program at Los Alamos National Laboratory, under the Office of Engineering and Technology Maturation. LA-UR-24-30342.

References

1. Fickenwirth, P. (2023). Electrodynamic Shaker Capability Estimation Through Experimental Dynamic Substructuring [Thesis]. https://doi.org/10.2172/1958984
2. Lang, G. F., and Snyder, D. (2001). Understanding the physics of electrodynamic shaker performance. Sound and vibration, 35(10), 24-33.
3. Schultz, R. (2019). Calibration of shaker Electro-Mechanical models. Proceedings of the 38th IMAC, https://www.osti.gov/biblio/1642863
4. Tiwari, N., Puri, A., and Saraswat, A. (2017). Lumped parameter modelling and methodology for extraction of model parameters for an electrodynamic shaker. Journal of Low Frequency Noise, Vibration and Active Control, 36(2), 99-115.
5. Martini, Luca. (2016). Real-time control of an Electrodynamic Shaker. Master's thesis, Alma Mater Studiorum - Università di Bologna,. http://amslaurea.unibo.it/10080/.
6. Adam, Caroline. (2022) Virtual Shaker Testing: Modelling, vibration analysis, and experimental validation of an electrodynamic shaker model coupled to a test specimen[BR]- Integration Internship. MatheO - Master Thesis Online matheo.uliege.be/handle/2268.2/14589.
7. Unholtz-Dickie Corporation (2018). H560 Operating and Maintenance Manual.
8. How to normalize the RMSE. (2019, January 7). https://www.marinedatascience.co/blog/2019/01/07/normalizing-the-rmse/
9. Tuman, M.J., Behling, M., Allen, M.S. et al. (2024). Balancing Impedance and Controllability in Response Reconstruction with TS-IMMAT. Exp Tech 48, 51–68. https://doi.org/10.1007/s40799-023-00645-1